ACS OMEGA

Article

http://pubs.acs.org/journal/acsodf

Inverse Moth Eye Nanostructures with Enhanced Antireflection and Contamination Resistance

Zhaolu Diao,[†,‡] Johannes Hirte,[†,‡] Wenwen Chen,[†,‡] and Joachim P. Spatz*[,†,‡]

[†] Department of Cellular Biophysics, Max Planck Institute for Medical Research, Jahnstraße 29, D-69120 Heidelberg, Germany

[‡] Department of Biophysical Chemistry, University of Heidelberg, INF 253, D-69120 Heidelberg, Germany

ABSTRACT: Moth-eye-inspired nanostructures are highly useful for antireflection applications. However, block copolymer micelle lithography, an effective method to prepare moth eye nanopillars, can only be used on a limited choice of substrates. Another drawback of nanopillar substrates is that contamination is easily absorbed, thereby reducing transmittance. The production of antireflective surfaces that are contamination-resistant or that can be cleaned easily without the loss of optical properties remains challenging. Here, we describe an approach for creating inverse moth eye nanostructures on other optical substrates than the most commonly used fused silica. We demonstrate its feasibility by fabricating a borosilicate substrate with inverse nanostructures on both sides. The etching of nanoholes on both sides of the substrate improves its transmittance by 8%, thereby surpassing the highest increase of transmittance yet to be obtained with nanopillars on fused silica. More importantly, the substrate with inverse moth eye nanostructures is more robust against contaminations than the substrates with nanopillars. No significant decrease in performance is observed after five cycles of repeated contamination and cleaning. Our approach is transferable to a variety of optical materials, rendering our antireflection nanostructures ideal for applications in touch devices such as touch screens and display panels.

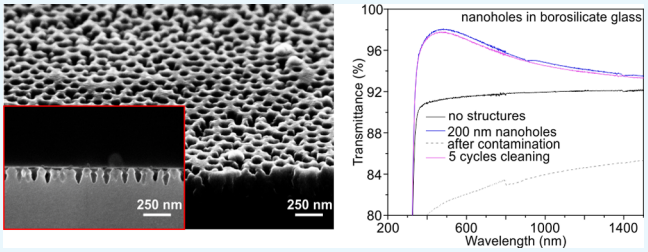

INTRODUCTION

Various concepts and techniques have been developed to overcome Fresnel reflection at the interface of materials with different refractive indices, among them moth-eye-inspired nanostructures with a gradient refractive index that can eliminate Fresnel reflection for omnidirectional incidence over a broad wavelength range.[1−4] Electron-beam lithography and interference lithography have been used in the past to fabricate such nanostructures. These methods, however, are unattractive because of their high cost and/or limited resolution.

More recently, block copolymer micelle lithography (BCML) and reactive ion dry etching have been used to prepare moth eye nanostructures on fused silica to achieve perfect transmission and zero reflection.[5,6] Unfortunately, the transferability of this method to other substrates is limited because the choice of the masking material for the BCML etching mask is restricted to gold, silver, platinum, and palladium.[7−10] This constitutes a problem because the selectivity of the etching process when, for instance, using gold or silver nanoparticles as the masking material is not sufficient to etch moth eye nanopillars into most types of suitable substrates. Therefore, the production of most kinds of optical glasses or materials with differing refractive indices or other desired optical properties entails costly, high-performance antireflection treatment. Moreover, nanopillars on the fused silica substrate, though relatively robust to mechanical damage, are very sensitive to contaminations through contact, such as fingerprints, and they are difficult to be cleaned.[11] Therefore, there exists a high demand to develop a new method to prepare antireflection nanostructures on a broader range of different types of optical materials. To this day, antireflection properties in combination with contamination resistance or easy clean ability remain far behind application requirements.

Inverse moth eye nanostructures, also called nanoholes, have been investigated regarding their antireflection, antimicrobial, and/or high damage tolerance properties.[11,12] Generally, these studies have concluded the greatest limitations of nanoholes to be the highly elaborate fabrication steps necessary for their production or their poor optical performance.[13−18] In this work, we developed a new method to convert a gold nanoparticle etching mask produced by BCML into an inverse chromium etching mask. This mask is used to etch semi-hexagonal nanoholes onto both sides of a borosilicate substrate. Nanoholes are expected to offer antireflection properties similar to those of nanopillars. Because of their geometry and high mechanical stability, they are also likely to have improved contamination resistance and to be easier to clean.[19]

RESULTS AND DISCUSSION

A schematic illustration of the process for realizing inverse moth eye nanoholes as well as the matching atomic force

Received: July 16, 2017
Accepted: August 9, 2017
Published: August 28, 2017

DOI: 10.1021/acsomega.7b01001
ACS Omega 2017, 2, 5012−5018

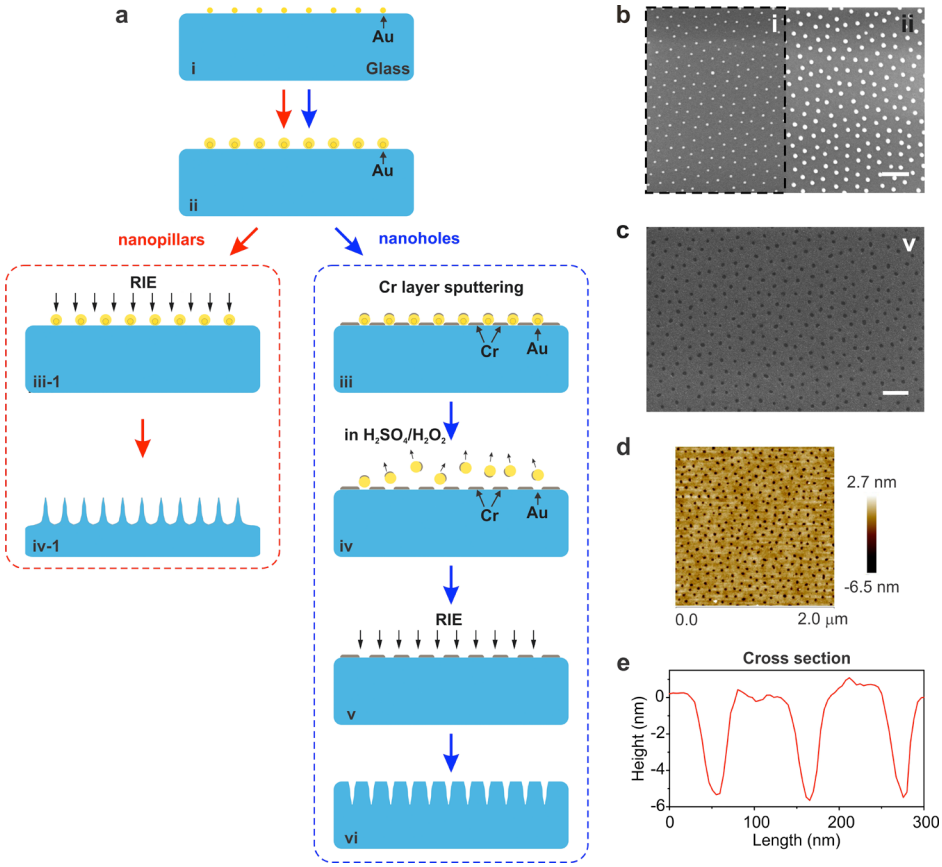

Figure 1. Fabrication of the nanohole and nanopillar substrates. (a) Diagram illustrating the production process: (i) a quasihexagonal array of gold particles is prepared on a glass substrate by BCML; (ii) the gold particles are enlarged by electroless deposition; (iii-1,iv-1) the enlarged gold particles are used as an RIE mask to create nanopillars; (iii) a thin layer of chromium is deposited on the surface by an e-beam sputter; and (iv,v) the gold nanoparticles are removed by treatment with piranha solution (H_2SO_4 (98%)/H_2O_2 (30%) = 3:1). The inverse chromium layer is used as an RIE mask to produce nanoholes. (b) Left: SEM image of a sample prepared by BCML (matching image to i). Interparticle spacing: 105 ± 4.7 nm; diameter: 7.0 ± 0.2 nm. Right: SEM image of the sample after electroless deposition (matching image to ii). Interparticle spacing: 105 ± 4.7 nm; diameter: 20.5 ± 0.8 nm. (c) SEM image after the removal of gold nanoparticles (matching image to v). (d) AFM image of the sample shown in (c). (e) Cross-sectional measurement of the sample shown in (d). (The thickness of the chromium layer is 5.5 ± 0.4 nm, and the distance between the holes in the chromium layer is 105 ± 4.7 nm.) The scale bar in (b,c) is 250 nm.

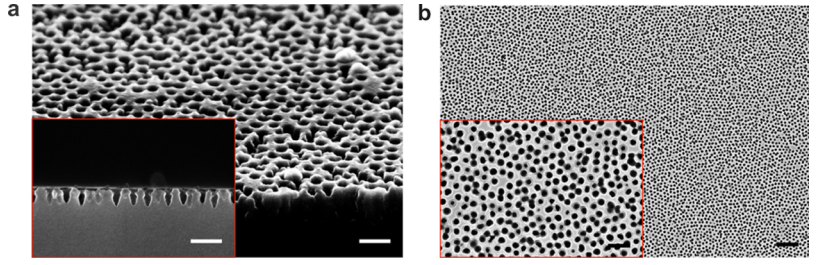

Figure 2. SEM images of nanoholes in the borosilicate glass substrate. (a) Tilted top-view (25° tilt) SEM image of the nanoholes. The inset shows a side view of the nano holes. The size of the scale bar in both is 250 nm. (b) Top-view SEM image of the nanoholes (scale bar = 2 μm). The inset shows an enlarged image (scale bar = 250 nm).

microscopy (AFM) and scanning electron microscopy (SEM) images is shown in Figure 1. A quasihexagonal pattern of gold nanoparticles is prepared by BCML on both sides of a borosilicate substrate. The interparticle distance is chosen to be 105.0 ± 12.0 nm, and the nanoparticles have a diameter of 7.0 ± 0.2 nm. The same parameters are also used for the nanopillars which will be discussed in this work. First, the diameter of the gold nanoparticles is increased to 20.5 ± 0.8 nm through an electroless deposition step. The growth of the gold nanoparticles is important to achieve ideal chromium coverage as this will later facilitate the removal of the gold particles. After the growth of the particles, a 5 nm chromium layer is sputtered onto the substrate. The thickness of the chromium layer is chosen such that chromium covers only the surface between the gold nanoparticles and the top of the gold particles. The sides of the gold particles remain uncovered. Immersion in piranha solution (H_2O_2 30% to H_2SO_4 98%, volume ratio 1:3) for two cycles of 5 min each removes the gold nanoparticles from the surface, leaving the chromium layer with holes where the gold particles were located before. As shown in

DOI: 10.1021/acsomega.7b01001
ACS Omega 2017, 2, 5012−5018

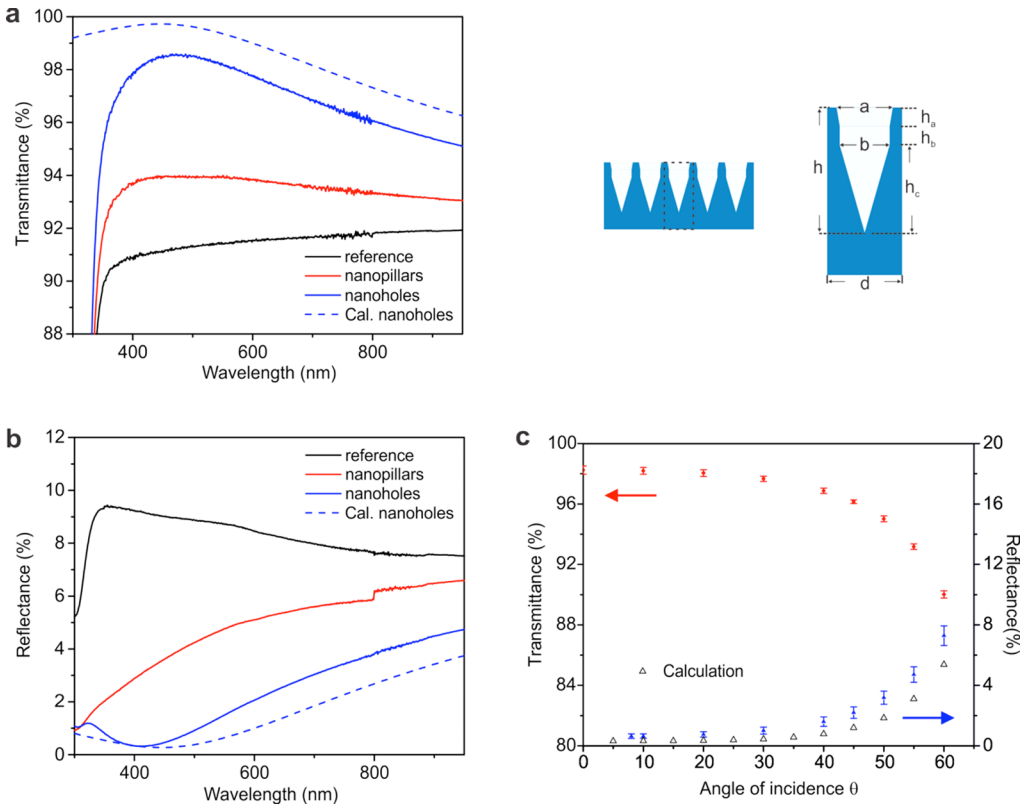

Figure 3. Transmittance and reflectance of a borosilicate glass substrate with nanoholes or nanopillars on both sides. (a,b) Comparison of the transmittance and reflectance (300−950 nm) of a borosilicate glass substrate with 200 nm nanoholes on both sides (in blue), a borosilicate glass substrate with 120 nm nanopillars on both sides (in red), and the reference sample without nanostructures (in black). The calculated transmittance and reflectance of the substrate with 200 nm nanoholes are in dashed red and blue curves. Parameters of nanoholes in calculation: h = 200 nm, d = 105 nm, a = 90 nm, b = 80 nm, $h_a = h_b$ = 30 nm, and h_c = 140 nm. (c) Measured average (380−500 nm) transmittance (red circles), reflectance (blue triangles), and calculated reflectance (black triangles) of the borosilicate glass substrates with 200 nm nanoholes on both sides shown in (a,b) measured at different angles of incidence.

Figure 1d,e, the chromium layer between the holes has an average thickness of 5 nm. Nanoholes with 200 nm depth are then etched into the borosilicate substrate using a reactive ion etching (RIE) machine. Finally, the chromium layer is removed using a chromium etcher.

Our new method successfully converts the gold nanoparticle etching mask into an etching mask of another material (chromium in this case), which features the inverse pattern. The dry etching selectivity of chromium to borosilicate glass is much higher than that of gold to borosilicate. Thus, the 5 nm chromium layer is very thick to allow the etching of nanoholes with a depth of 200 nm. Other materials that cannot be etched using a gold nanoparticle etching mask may also be suitable for this method. Figure 2 shows SEM images of the nanoholes. These holes differ from the nanopillars we published in an earlier work in two major ways.[6] Compared to the previously described nanopillars, the sidewall of the nanoholes is more slanted. The borosilicate glass contains silicon dioxide (60−70%) and different weight contributions of Al_2O_3, B_2O_3, K_2O, and Na_2O.[20] These components have a high chemical resistance and a very low thermal expansion coefficient. As a result, they make borosilicate glass more resilient to be etched than fused silica. The top-view diameter of the nanoholes differs from the diameter of the nanopillars made using the original gold nanoparticle etching mask (Figure 2b). This is related to the fact that the thickness of the chromium layer is the thinnest at the edge of each hole and gets thicker as it is further from the edge. The thinner the chromium layer is, the faster it is etched away. Thus, the thin layer of chromium surrounding the holes' edges causes the nanoholes to have an inverted cone shape (wider top and narrower bottom). Fortunately, these two differences (larger circumference and cone shape) between the nanopillars and the nanoholes do not interfere with the antireflective properties of the nanostructured surface, as the gradient refractive index change from the surrounding air to the glass is not affected.

We used our new nanohole etching method to prepare nanoholes on both sides of a borosilicate substrate. The transmittance and reflectance of this substrate were then compared to a borosilicate substrate structured with nanopillar-like structures on both substrate sides (using the original gold nanoparticle etching mask) as well as a borosilicate reference substrate without nanostructures. The first two were etched using the inverse chromium etching mask (to produce nanoholes) or the original gold dot etching mask (to produce nanopillars) over an identical number of cycles in a RIE machine (details described in Experimental Section or Computational Methods). The 200 nm sized nanoholes on the structured surfaces produce a gradient refractive index change from the air to the substrate. The maximum transmittance is 98.9% at a wavelength of 490 nm. Our attempts to etch nanopillars into the borosilicate substrate using the gold particle mask were unsuccessful because of the different components in the borosilicate glass. These

DOI: 10.1021/acsomega.7b01001
ACS Omega 2017, 2, 5012−5018

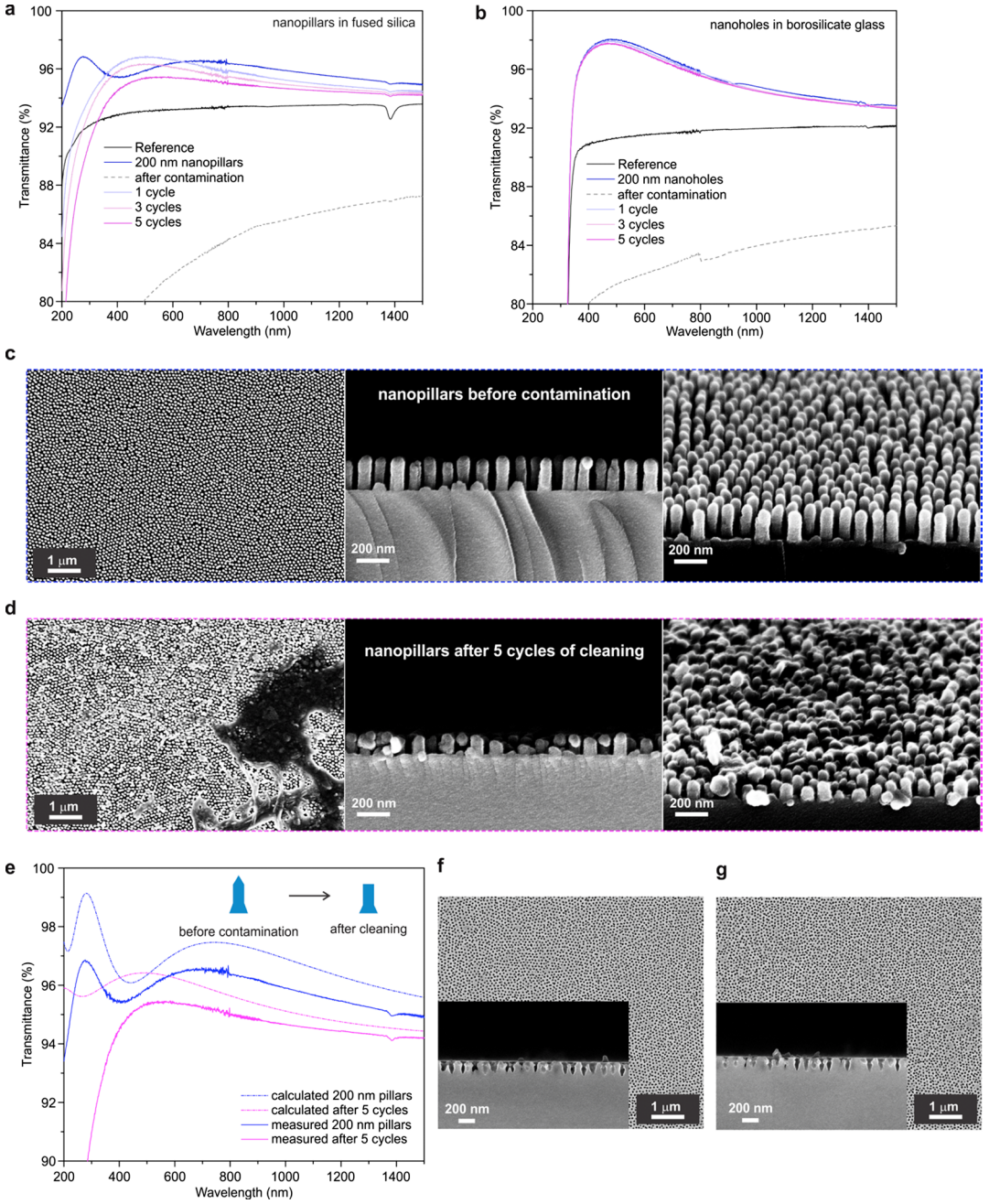

Figure 4. Transmittance of a fused silica nanopillar substrate and a borosilicate nanohole substrate after repeated contamination and cleaning. (a) Transmittance of the fused silica substrate with 200 nm nanopillars on both sides (in blue). The transmittance of the sample after the initial fingerprint contamination (in dashed gray); after 1, 3, or 5 repeated cycles of both fingerprint contamination and cleaning (in light blue, light purple, and purple, respectively). (b) Transmittance of the borosilicate glass substrate with 200 nm nanoholes on both sides (in blue). The transmittance of this sample after the initial fingerprint contamination (in dashed gray); after 1, 3, or 5 repeated cycles of both fingerprint contamination and cleaning (in light blue, light purple, and purple, respectively). (c) SEM images of 200 nm nanopillars before contamination (from left to right: top view, side view, and tilted top view). (d) SEM images of 200 nm nanopillars after five cycles of contamination and cleaning (from left to right: top view, side view, and tilted top view). (e) Measured (solid curves) and calculated (dashed curves) transmittance of 200 nm nanopillars on fused silica before contamination (blue curves) and after five cycles of cleaning and contamination (purple curves). (f) Top-view SEM image of 200 nanoholes before contamination (inset: side view). (g) Top-view SEM image of 200 nanoholes after five cycles of contamination and cleaning (inset: side view).

components possess a low etching selectivity compared to the gold dot etching mask. Thus, the gold dots are etched away at the beginning of the etching process, resulting in pillarlike random nanostructures with limited height (less than 120 nm in height) on the surface. Shown as the red curve in Figure 3a, the transmittance of this substrate is only 2 to 3% higher than that of the unstructured control substrate. Because of the limited height of the nanopillars, transmittance reaches a limited maximum at a short wavelength of 395 nm. Figure 3b shows the reflectance of the substrates. Much like the transmittance, the minimum reflectance of the nanohole substrate (0.3% at 460 nm) is also lower than that of the nanopillar substrate. Figure 3c shows the transmittance and reflectance of the nanohole substrate at different angles of

DOI: 10.1021/acsomega.7b01001
ACS Omega 2017, 2, 5012−5018

incidence. At angles of incidence up to 30°, the nanohole substrate has good antireflection properties. At angles of incidence exceeding 30°, the reflectance increases significantly. This also agrees well with calculation results, as shown in the black triangle in Figure 3c.

A comparison of the optical properties of the borosilicate nanohole substrate and a fused silica nanopillar substrate (produced as described in a previous publication[6]) shows that the maximum transmittance of the nanohole substrate (98.9%) is lower than that of the nanopillar substrate (pillar spacing 105 nm, height 450 nm, and maximum transmittance 99.8%). However, the absolute improvement in transmittance (compared to a nonstructured substrate) for the nanohole substrate (8% at its maximum, from 90.9 to 98.9% for a borosilicate substrate) is much higher than that of the nanopillar substrate (6.8% at its maximum, from 93 to 99.8% for a fused silica substrate). This demonstrates that this new method to prepare nanoholes represents an improvement. On the basis of the result of the calculation, as shown in the dashed blue curves in Figure 3a,b, the antireflection property of these nanoholes can be further optimized. It can be expected that optimizing the geometry and/or reducing the surface roughness of the holes will further improve the transmittance of the nanohole substrate.

Despite their outstanding antireflection properties, moth-eye-inspired nanostructures have two main disadvantages. The first is their high preparation cost because of elaborate fabrication procedures. This restriction can be solved by utilizing BCML for the production of the nanopillars or nanoholes. Second, these nanostructures are easily contaminated during experimental handling. Furthermore, an efficient method to clean these substrates and to restore their antireflection function has not yet been reported and would represent a breakthrough improvement for practical applications. On the basis of their geometry, we expect nanoholes to be more resistant to contaminations and more robust during cleaning than the nanopillars.[21] To look at this in greater details, we compared the tolerance of the nanopillars and nanoholes to surface cleaning. Many types of contaminations exist. Here, we focused on the effect of fingerprint contacts. We compared the effect of multiple fingerprint contaminations and cleaning steps on a fused silica SUPRASIL substrate featuring 200 nm high nanopillars on both sides and a borosilicate glass substrate with 200 nm deep nanoholes on both sides. As shown in Figure 4a,b, the transmittance of both substrates decreases strongly after fingerprint contamination (dashed gray curves). This is a 15% decrease compared to transmittance before the contamination. Next, we cleaned both substrates following an identical protocol using Hellmanex solution. We repeated this combination of fingerprint contamination and cleaning steps up to five times. Transmittance measurement after five rounds of contamination and cleaning revealed two effects (see Figure 4a): the maximum transmittance of the nanopillar substrate shifts toward a longer wavelength range and it decreases by more than 1.5%. In comparison, the transmittance of the nanohole substrate—with a maximum decrease of less than 0.2%—remains almost unchanged after five rounds of contamination and cleaning. This proves that the nanoholes' antireflection properties are more robust against repeated contamination and cleaning than the nanopillars' transmittance. To understand the mechanism of the contamination and cleaning process, we check the substrate with 200 nanopillars by a scanning electron microscope. As shown in Figure 4c, the nanopillars have a round tip and a homogeneous height before the contamination and cleaning steps. After five cycles of contamination, as shown in Figure 4d, the tips of the nanopillars are damaged or distorted with some residual contamination on top. On the basis of the SEM image of the side view, most of the nanopillars have flat top surface. During these cycles, some of the nanopillars are broken at different heights with an increasing variation of pillar height. All these key differences before and after cleaning are considered in the simulation shown in Figure 4e. The maximum transmittance of the nanopillar after cleaning (purple dashed curve) shifts toward a longer wavelength range, and it decreases by more than 2.5%. However, as shown in Figure 4f,g, the shape of the nanoholes is almost not changed during the same treatment. The geometry of the nanopillars is much more sensitive to the contamination and cleaning processes than that of the nanoholes. It can be concluded that the nanoholes are better suited for antireflection interfaces that need to be contamination-resistant or easy for cleaning.

CONCLUSIONS

We have developed a new method to prepare inverse moth eye structures on materials other than fused silica. An increase of transmission of more than 8% is observed on a borosilicate glass substrate with nanoholes on both sides. New possibilities for transferring the method to other materials have emerged through expanding the original BCML nanolithography method based on a gold nanoparticle etching mask to include a second inverse chromium mask after electroless deposition. Possible materials include optical glass with a high refractive index and optical materials that cannot be etched with a gold etching mask. An additional advantage is the possibility to clean these nanohole substrates multiple times without significantly damaging their antireflection properties. We believe that this novel method will open new doors for preparing moth eye/inverse moth eye nanostructures on a wide range of previously unusable optical materials. Our technique creates new possibilities for applications that require high contamination resistance and/or must be easy to clean.

EXPERIMENTAL SECTION OR COMPUTATIONAL METHODS

BCML was employed to create a hexagonal pattern of gold nanoparticles on the fused silica or borosilicate substrates. Polystyrene-*block*-2-vinylpyridine or PS-*b*-P2VP (M_n (PS) = 110 000, M_n (PVP) = 70 500, M_w/M_n = 1.09, Polymer Source Inc.) copolymers were dissolved in *o*-xylene at a concentration of 4 mg/mL and stirred for 24 h to form micelles. Gold salt ($HAuCl_4 \cdot 3H_2O$, MW = 393.83 g/mol, Sigma-Aldrich) was added with a loading rate (L) of 0.25. The substrates were spin-coated at 7000 rpm for 60 s to create the hexagonal pattern. The gold nanoparticles were grown by electroless deposition. First, the substrates were activated by hydrogen plasma treatment (3 min, 0.4 mbar, and 200 W) using a PVA TePla 1000 microwave system. The activated substrates were dipped into a solution of 0.1% $HAuCl_4$/0.4 mM HN_3OHCl for 30 s. The polymer shell was then removed by a second hydrogen plasma treatment (10 min, 0.4 mbar, and 350 W). The hexagonal gold nanoparticle pattern on a fused silica substrate was used as an etching mask for the RIE of nanopillars.

The hexagonal gold nanoparticle array on a borosilicate substrate was further used to create an inverse chromium

DOI: 10.1021/acsomega.7b01001
ACS Omega 2017, 2, 5012−5018

etching mask for the production of a hexagonally arranged nanohole pattern. To this end, a GLAD system (homebuilt e-beam evaporator) was used (10 kV, 15 mA, 1.5×10^{-6} mbar) to sputter a 5 nm thick layer of chromium with a sputter rate of 0.3 Å/s onto the hexagonal gold nanoparticle array. Prior to RIE, the gold nanoparticles were removed by immersing the substrates in freshly prepared piranha solution (consisting of 1 part 30% p.a. hydrogen peroxide solution and 3 parts 98% sulfuric acid) for 5 min and subsequent rinsing with ultrapure water. An Oxford PlasmaLab 80 RIE etcher was used to etch the hexagonal nanohole pattern into the borosilicate substrate. Two different etching steps were used to control the geometry and refractive index profile of the nanopillars. The first etching step consisted of two treatments: first with a 1:1 mixture of Ar and SF_6 [80 sccm, 50 mTorr, radio frequency (rf) power 120 W, 60 s] and followed by a treatment with a 1:1 mixture of Ar and CHF_3 (80 sccm, 50 mTorr, rf power 120 W, ICP power 20 W, 20 s). The second etching step consisted of a single treatment with a 1:1 mixture of Ar and SF_6 (80 sccm, 50 mTorr, rf power 120 W, 80 s). Different cycles of these two steps were carefully combined until the desired structure depth was reached. The temperature of the sample was kept constant at 20 °C during the entire process.

A Cary 5000 Ultraviolet−visible−near-infrared spectrometer was used to measure the transmittance and reflectance (175−3300 nm) for comparing the borosilicate nanohole substrate, the fused silica nanopillar substrate, and the unstructured reference substrate. A specially designed OMT goniometer was used to determine the angle of incidence (380−1100 nm, transmittance 0−60°, reflectance 8−60°).

Fingerprints were applied on both sides of the substrate (with nanoholes or nanopillars) with pressure. Afterward, the contaminated samples were immersed into a 30 °C preheated Hellmanex III solution (Hellma Analytics, Müllheim, Germany) for 15 min. Then, the samples were thoroughly rinsed with deionized water and dried in a nitrogen stream. This procedure was repeated several cycles to test the long-term durability. After each contamination and cleaning step, the transmittance was measured.

An array of 100 nanoholes or nanopillars with the hole depth or pillar heights following a normal distribution was considered as a unit for the simulation. The filling factor in the unit was calculated layer-by-layer along the hole depth or pillar height in steps of 1 nm. The reflectance and transmittance were simulated by MATLAB (R2016a, MathWorks) based on the open-source thin-film toolbox developed by Griesmann (U. Griesmann, "Thin film tool box-Ulf's Cyber Attic"). Parameters of the nanopillars used in calculation for Figure 4e: Before contamination, height = 200 nm × (1 ± 5%), interpillar spacing = 105 nm, bottom width = 90 nm, middle width = 65 nm, height bottom/height = height top/height = 25%, and height middle/height = 50%. After five cycles of contamination, height = 150 nm × (1 ± 50%), interpillar spacing = 105 nm, bottom width = 90 nm, middle width = 65 nm, height bottom/height = 25%, and height middle/height = 75%.

AUTHOR INFORMATION

Corresponding Author

*E-mail: jspatz@mpimf-heidelberg.mpg.de (J.P.S.).

ORCID

Joachim P. Spatz: 0000-0003-3419-9807

Notes

The authors declare no competing financial interest.

ACKNOWLEDGMENTS

The research is partially supported by the BMBF funding for "NanoAR" (V.I.P 03V0438) project. J.P.S. is the Weston Visiting Professor at the Weizmann Institute of Science. The authors also thankfully acknowledge the general support of the Max Planck Society.

REFERENCES

(1) Clapham, P. B.; Hutley, M. C. Reduction of Lens Reflection by "Moth Eye" Principle. *Nature* **1973**, *244*, 281−282.

(2) Vukusic, P.; Sambles, J. R. Photonic structures in biology. *Nature* **2003**, *424*, 852−855.

(3) Xi, J.-Q.; Schubert, M. F.; Kim, J. K.; Schubert, E. F.; Chen, M. F.; Lin, S.-Y.; Liu, W.; Smart, J. A. Optical thin-film materials with low refractive index for broadband elimination of Fresnel reflection. *Nat. Photonics* **2007**, *1*, 176−179.

(4) Buencuerpo, J.; Torné, L.; Álvaro, R.; Llorens, J. M.; Dotor, M. L.; Ripalda, J. M. Nano-cones for broadband light coupling to high index substrates. *Sci. Rep.* **2016**, *6*, 38682.

(5) Lohmüller, T.; Helgert, M.; Sundermann, M.; Brunner, R.; Spatz, J. P. Biomimetic interfaces for high-performance optics in the deep-UV light range. *Nano Lett.* **2008**, *8*, 1429−1433.

(6) Diao, Z.; Kraus, M.; Brunner, R.; Dirks, J.-H.; Spatz, J. P. Nanostructured Stealth Surfaces for Visible and Near-Infrared Light. *Nano Lett.* **2016**, *16*, 6610−6616.

(7) Spatz, J. P.; Mössmer, S.; Hartmann, C.; Möller, M.; Herzog, T.; Krieger, M.; Boyen, H.-G.; Ziemann, P.; Kabius, B. Ordered deposition of inorganic clusters from micellar block copolymer films. *Langmuir* **2000**, *16*, 407−415.

(8) Glass, R.; Möller, M.; Spatz, J. P. Block copolymer micelle nanolithography. *Nanotechnology* **2003**, *14*, 1153−1160.

(9) Wilcoxon, J. P.; Abrams, B. L. Synthesis, structure and properties of metal nanoclusters. *Chem. Soc. Rev.* **2006**, *35*, 1162−1194.

(10) Lohmueller, T.; Bock, E.; Spatz, J. P. Synthesis of quasi-hexagonal ordered arrays of metallic nanoparticles with tuneable particle size. *Adv. Mater.* **2008**, *20*, 2297−2302.

(11) Vogel, N.; Belisle, R. A.; Hatton, B.; Wong, T.-S.; Aizenberg, J. Transparency and damage tolerance of patternable omniphobic lubricated surfaces based on inverse colloidal monolayers. *Nat. Commun.* **2013**, *4*, 2176.

(12) Kim, J.-G.; Choi, H. J.; Park, K.-C.; Cohen, R. E.; McKinley, G. H.; Barbastathis, G. Multifunctional Inverted Nanocone Arrays for Non-Wetting, Self-Cleaning Transparent Surface with High Mechanical Robustness. *Small* **2014**, *10*, 2487−2494.

(13) Brieger, S.; Dubbers, O.; Fricker, S.; Manzke, A.; Pfahler, C.; Plettl, A.; Ziemann, P. An approach for the fabrication of hexagonally ordered arrays of cylindrical nanoholes in crystalline and amorphous silicon based on the self-organization of polymer micelles. *Nanotechnology* **2006**, *17*, 4991−4994.

(14) Byeon, K.-J.; Hwang, S.-Y.; Lee, H. Fabrication of nano-hole array patterns on transparent conducting oxide layer using thermally curable nanoimprint lithography. *Microelectron. Eng.* **2008**, *85*, 830−833.

(15) Li, S.; Yang, Z.; Zhang, Z.; Gao, F.; Du, J.; Zhang, S. Study of nanospheres lithography technology with super-lens for fabricating nano holes. *J. Appl. Phys.* **2013**, *113*, 183102.

(16) Wang, W.; Zhang, W.; Fang, X.; Huang, Y.; Liu, Q.; Bai, M.; Zhang, D. Omnidirectional light absorption of disordered nano-hole structure inspired from Papilio ulysses. *Opt. Lett.* **2014**, *39*, 4208−4211.

(17) Krishnamoorthy, S.; Pugin, R.; Brugger, J.; Heinzelmann, H.; Hoogerwerf, A. C.; Hinderling, C. Block copolymer micelles as switchable templates for nanofabrication. *Langmuir* **2006**, *22*, 3450−3452.

DOI: 10.1021/acsomega.7b01001
ACS Omega 2017, 2, 5012−5018

(18) Wen, L.; Xu, R.; Mi, Y.; Lei, Y. Multiple nanostructures based on anodized aluminium oxide templates. *Nat. Nanotechnol.* **2017**, *12*, 244−250.
(19) Mirotznik, M. S.; Good, B. L.; Ransom, P.; Wikner, D.; Mait, J. N. Broadband Antireflective Properties of Inverse Motheye Surfaces. *IEEE Trans. Antennas Propag.* **2010**, *58*, 2969−2980.
(20) Steiner, J. Schott,Otto and the Invention of Borosilicate Glass. *Glastech. Ber.* **1993**, *66*, 165−173.
(21) Tuteja, A.; Choi, W.; Mabry, J. M.; McKinley, G. H.; Cohen, R. E. Robust omniphobic surfaces. *Proc. Natl. Acad. Sci. U.S.A.* **2008**, *105*, 18200−18205.

DOI: 10.1021/acsomega.7b01001
ACS Omega 2017, 2, 5012−5018